Field measurements of cable self-burial in a sandy marine environment

Unsworth, Christopher; Austin, Martin; Van Landeghem, Katrien; Couldrey, Amelia; Whitehouse, Richard; Lincoln, Ben; Doole, Siobhan; Worrall, Peter

Coastal Engineering

DOI:
10.1016/j.coastaleng.2023.104309

Published: 01/09/2023

Peer reviewed version

Field measurements of cable self-burial in a sandy marine environment

Christopher A. Unsworth[1*], Martin J. Austin[1], Katrien J.J. Van Landeghem[1], Amelia J. Couldrey[2], Richard J.S. Whitehouse[2], Ben Lincoln[1], Siobhan Doole[3], Peter Worrall[3].

[1]School of Ocean Sciences, Bangor University, Menai Bridge, Isle of Anglesey LL59 5AB, United Kingdom.
[2]Coasts and Oceans, HR Wallingford, Kestrel House, Howbery Park, Wallingford OX10 8BA, United Kingdom.
[3]JDR Cables Victoria Dock, Greenland Rd, Hartlepool TS24 0RQ, United Kingdom.

* *Correspondence to*: Christopher A. Unsworth[1] (christopher.unsworth@bangor.ac.uk)

Abstract.

The world's shallow continental shelves are currently experiencing a rapid pace of development from the growth of offshore renewable energy. The emplacement of infrastructure on the seabed can change the morphology of the bed, the nature of the flow above it and transport of sediment and so complicate the assessment of seabed stability for planning and designing offshore renewable infrastructure. To ascertain how much of an impact these natural processes have on cable stability, we present the first field observations made directly over a section of subsea cable, from two deployments in the Eastern Irish Sea at a location of current and planned offshore windfarms. Profiles of flow, turbulence and suspended sediment concentration were measured over a section of typical high voltage electricity cable. Upon deployment our observations show that sediment was deposited around the cable and self-burial occurred. The rate of deposition varied between surveys dependent on forcing and local bed conditions. Turbulence generated from the cable itself reduced as the embedment depth increased, but the relationship between bed shear stress and suspended sediment concentration was not consistent between surveys. We discuss several processes potentially responsible for the prevalence of deposition around the cable, and the difference in seabed mobility between the surveys.

Highlights:

1. Repeated field surveys quantified mean flow, turbulence and suspended sediments around a section of seafloor electricity cable
2. Deposition around the cable occurred at all initial embedment depths, but rates of deposition varied between surveys
3. Seabed mobility appears to have varied between surveys beyond any reasonable variation in grain size, indicating a yet unquantified control on seabed mobility.

1 Introduction

The cables that underpin the transfer of energy and data across the sea floors are vulnerable to the impacts exerted by a mobile and dynamic seabed. The exposure and subsequent damage from fishing, anchors, or abrasion during sediment transport can disrupt communication and critical infrastructure. There are a number of risks to infrastructure stability in the marine environment, from excess burial of high voltage cables causing overheating and reduction in transmission capacity to sea floor scour and bedform migration leading to cable exposures. For offshore windfarms crucial to the green energy transition, power cable repair in the United Kingdom (UK) alone costs between £1.3M (per inter-array cable) and £27M (per export cable) and takes 40-60 days to complete. Subsequent loss claims are estimated to account for > 40 % of UK Offshore Renewable Energy (ORE) insurance claims. Cable claims make up 83% of all claim's costs, with vessel costs a major factor. Between 2014-17, cable failure led to a cumulative loss of power generation of ~2.45 TWh, equating to ~£250M (El Mountassir & Strang-Moran, 2018). Based on recent analysis 57 of the last 60 construction projects in the UK experienced cable failure, suggesting that occurrences and associated disruption and costs will increase as the number of windfarms and wind turbines increases over the next decade.

Cables can become exposed and suffer fatigue loading due to self-induced scour of the seabed, causing the cable to sag and vibrate when unsupported (Mayall et al., 2020; Sumer et al., 2001a,b; Zhang et al., 2021); a similar affect can happen due to the passing of bedforms, leading to local scour around a section of a cable (Couldrey et al., 2020; Damgaard et al., 2015). The onset of cable scour caused by uni-directional currents can be predicted using the cable's Shields type parameter (Sumer & Fredsøe, 2001; 2002);

$$\frac{\boldsymbol{U_{cr}^2}}{\boldsymbol{gD_c(1-n)(s-1)}} = \mathbf{0.025}\ \boldsymbol{exp}\left[\mathbf{9}\left(\frac{\boldsymbol{e_c}}{\boldsymbol{D_c}}\right)^{\mathbf{0.5}}\right] \qquad \text{Eq. 1}$$

where U_{cr} is the mean current required for the onset of scour under the cable, defined at the top of the cable and n is porosity of the seabed (= 0.4), g is acceleration due to gravity (assumed 9.81 m s^2), s is the relative density of sediment in water ($s = \rho_s/\rho_w$), D_c is the diameter of the cable and e_c is the embedment depth. Flows in mobile sedimentary environments less than the critical velocity for onset of scour should lead to deposition, with scour occurring once flows exceed the threshold (Figure 1).

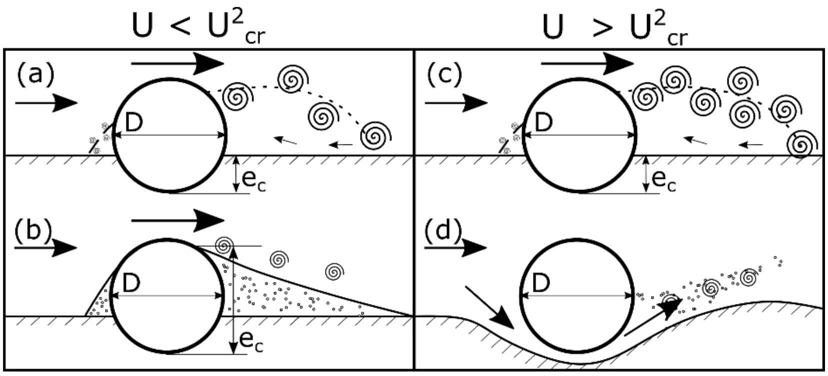

Figure 1. Conceptual diagram of cable-seabed interactions under different hydraulic and sediment regimes. (a) and (b) represent before and after responses to flow separation over a cable when $\boldsymbol{U < U_{cr}^2}$ the threshold outlined by Eq. 1. Whilst (c) and (d) represent what happens in the hydraulic regime.

Whilst seabed mobility is often included in the design and placement of seafloor cables around offshore windfarms, it is unclear why cables will either scour or self-bury through natural marine processes (Whitehouse & Draper, 2020). One possible cause could be the turbulence generated by the cables themselves -which depending on the environmental conditions will either induce erosion or deposition of sediment around the cable. Such morphological alternation of the local environment by the cable itself is often not included in an assessment of cable stability at the site as cable design is often concerned with cable scour through piping, tunnel scour and liquefaction (Sumer & Fredsøe, 2001; Sumer & Kirca, 2022). Recent field surveys have revealed that cables and pipelines can self-bury due to the drag on the flow acting as a sediment attractor (Leckie et al., 2016), and not just as a cause of scour (cf. Sumer et al., 2001a). There are examples where high levels of suspended sediment will result in deposition, rather than erosion and scour, even when the hydraulic conditions would otherwise indicate scour formation (Leckie et al., 2018; Zhao et al., 2015), suggesting that additional processes need to be accounted for when estimating the onset of scour.

In a highly mobile environment, it is difficult to define the range of conditions a cable may experience due to the varying scales of induced turbulence from the infrastructure itself and from the passage of migrating bedforms; both can affect the reference velocity used to estimate the potential for scour (Couldrey et al., 2020). Turbulence and mean velocity can change dramatically over a single bedform – greatly affecting shear and bed shear stress at a local (metre) scale (Bennett & Best, 1995; Dey et al., 2020; Unsworth et al., 2018). The overall bed mobility can also change spatially over sub-tidal bedforms due to biological modification of the seabed (Damveld et al., 2018) or via the reversing tidal flow mobilising sediment just at bedform crests (Lefebvre et al., 2022), which further complicates prediction of seabed mobility and sediments response to the induced turbulence from offshore infrastructure. Waves also have a moderating effect on scour, but also on near bed suspended sediment concentration and seabed cohesion, adding a temporal (through storms) and spatial (location of the wave base) variability to their effects on the seabed. Much of the laboratory work which underpins cable-seabed interaction has focused on identifying the onset of scour (Sumer et al., 2001a; Sumer & Fredsøe, 2001, 2002) rather than the morphodynamics induced by periodic tidal conditions (Leckie et al., 2016). Yet, the dynamic feedbacks between flow, the suspension of sediment, and deposition around the cable (Leckie et al., 2015, 2016, 2018). For example, deposition around the cable and increasing embedment depth (e_c) creates positive feedback which reduces the amount of induced turbulence shed from the cable – and subsequently decreases the likelihood of scour. Clearly, field surveys are needed to see how the natural complexity of these environments can affect our present understanding of cable scour processes, particularly the time-dependent nature of these processes.

The aim of this paper is to quantify what role seabed mobility, suspended sediment concentration and locally produced turbulence have on modifying the existing relationships for the prediction of cable scour. We hypothesise: (1) that the turbulence and sediment suspension induced from offshore renewable infrastructure can alter these relationships; and (2) that high levels of suspended sediments found in tidally energetic environments promote deposition, rather than erosion, around cables (Figure 1). We use field observations made in a shallow tidally energetic environment to quantify both the flow and sediment dynamics over a section of subsea cable using multiple acoustic profiling instruments. We take advantage of different flood and ebb flow regimes caused by the careful design and deployment of our instrument lander to quantify the impact of the self-generated lee wake on the mean and turbulent flows across the cable and their subsequent control on cable burial.

The paper is organised as follows. After brief reviews of the field site and methods (Section 2), we present the results (Section 3). This is followed by sections based on more detailed analysis of the data (Section 4), which focuses on the effect of varying embedment depth on: (1) exploration of the timing of bed level changes around the cable, (2) the hydraulic conditions the cable experienced in relation to Eq.1 and (3) the effects of drag and turbulence produced the cable. The paper concludes with a discussion and summary of the results.

2.1 Methods, field site, and deployment

2.1.1 The study site

The study site was on the *Constable Bank* in the Irish Sea 6 km off the coast of North Wales, UK (53° 22.5616’ N, 3° 43.6308’ W, Figure 2). The site is close to existing and proposed offshore windfarms and their cables, so the surveys are highly representative of the active and future offshore renewable energy environment. The site has a semi-diurnal macro tidal regime, mean tidal ranges of 7.2 m at springs and 3.8 m at neaps (measured at *Llandudno*, https://ntslf.org). The tidal wave is standing, and dominant flood and ebb directions (from North) are 100° and 270 – 290°, respectively, with directions typically more consistent during floods than ebbs, as rotation of flow at slack tide lags due to the inertia of flow into Liverpool Bay. Median wave heights measured from the Rhyl Flats wave rider (coastalmonitoring.org) over the period 2007 – 2021 are 0.57 m, with 90th and 99th percentile significant wave heights of 1.39 m and 2.42 m, respectively. Significant wave periods are typically short, with a median of 4 s, and 6.7 s at the 99th percentile. Dominant wave directions are between 300° and 350°, with a maximum fetch of 160 km.

2.1.2 The data collected

The project saw two offshore surveys of the Constable Bank (Table 1), during which a seabed lander was deployed, and seabed bathymetry data was continuously collected using a vessel mounted Multibeam Echosounder (MBES) over the lander site. In the 2020 deployment the lander was positioned twice to try and gain repeated measurements of the initial flow and sediment transport response to the lander being positioned on the seabed. The 2021 survey was only one deployment, for a longer time period.

Table 1. Dates of surveys.

Dates	Location of the lander
18/9 -> 19/9/2020	Lat: 53° 22' 32.3295 Lon: -3° 43' 36.0741
20/9 -> 23/9/2020	Lat: 53° 22' 32.7459 Lon: -3° 72' 34.8921
14/7 -> 18/7/2021	Lat: 53° 22' 33.9122 Lon: -3° 43' 39.9091

Figure 2d-e provides a close-up of the seabed morphology as measured during the lander deployments and inset of the outline of the lander as seen by the MBES. The seabed lander, fitted with instrumentation as well as a section of seabed electricity cable (diameter D_c = 200 mm), was deployed from the RV Prince Madog at the end of an ebb tide. The front end of the lander supporting the cable faced into the dominant flood direction so that data collected during flood tide measured the natural flow (unaffected by the presence of the cable or lander), whilst data collected during ebb tides would be measuring the self-generated turbulent wake from the lander and cable (Figure 3). Instrumentation setup details relevant to the current study are given in Table 2. Seabed sediment grain size distribution was measured from analysing Shipek grab samples collected immediately prior to deployment of the lander in 2021. Samples were washed and dried overnight at 80°C and dry sieved and weighed following the British Standard protocol (BS1377), with fines (< 63 μm) collected onto pre-weighed filter paper, dried and weighed. Summary data are given in Table 3, with full details in appendix Table S1. Grain sizes are very consistent between surveys, with a 2 μm difference in median grain size. The ends of the distribution (D_{10} and D_{90}) are slightly boarder in 2020 than 2021, but well within the same fine to median sand size range. The percentage of fines (< 63 um) is higher in the 2021 survey, but still less than 1% of the sample mass, indicating that there was little to no effect on sediment threshold of motion due to fines (Mohr et al, 2016) in either survey.

Table 2. Instruments deployed and setup information.

Instrument	Orientation	Mounting elevation	Vertical bin height	Measurement frequency	Burst length (Rest interval)
Nortek AWAC (600 kHz)	Upward facing	1.5 m	1 m	1 Hz (currents and waves)	Currents: 1 min (10 min) Waves: 8.5 min (20 min)
Nortek Signature ADCP (1 MHz)	Upward facing	1.4 m	0.5 m	8 Hz	10 minutes (30 minutes)
2x Nortek Aquadopp (1 MHz)	Downward Facing	1.13 m	0.05 m	2 Hz	10 minutes (30 minutes)
Aquatec Aquascat (ABS) 2020 : 1, 2, 4, 5, MHz 2021 : 1, 2, 2.25, 4, MHz	Downward Facing	0.85 m	2020: 0.01 m 2021: 0.005 m	64 Hz, internally averaged to 4 Hz	10 minutes (30 minutes)

Table 3. Summary data from bed sediment samples

	2020	2021

% of samples < 0.063 µm by dry weight	0.09 %	0.22 %
D_{10} (µm)	188	196
D_{16} (µm)	201	211
D_{50} (µm)	243	245
D_{84} (µm)	281	271
D_{90} (µm)	293	279

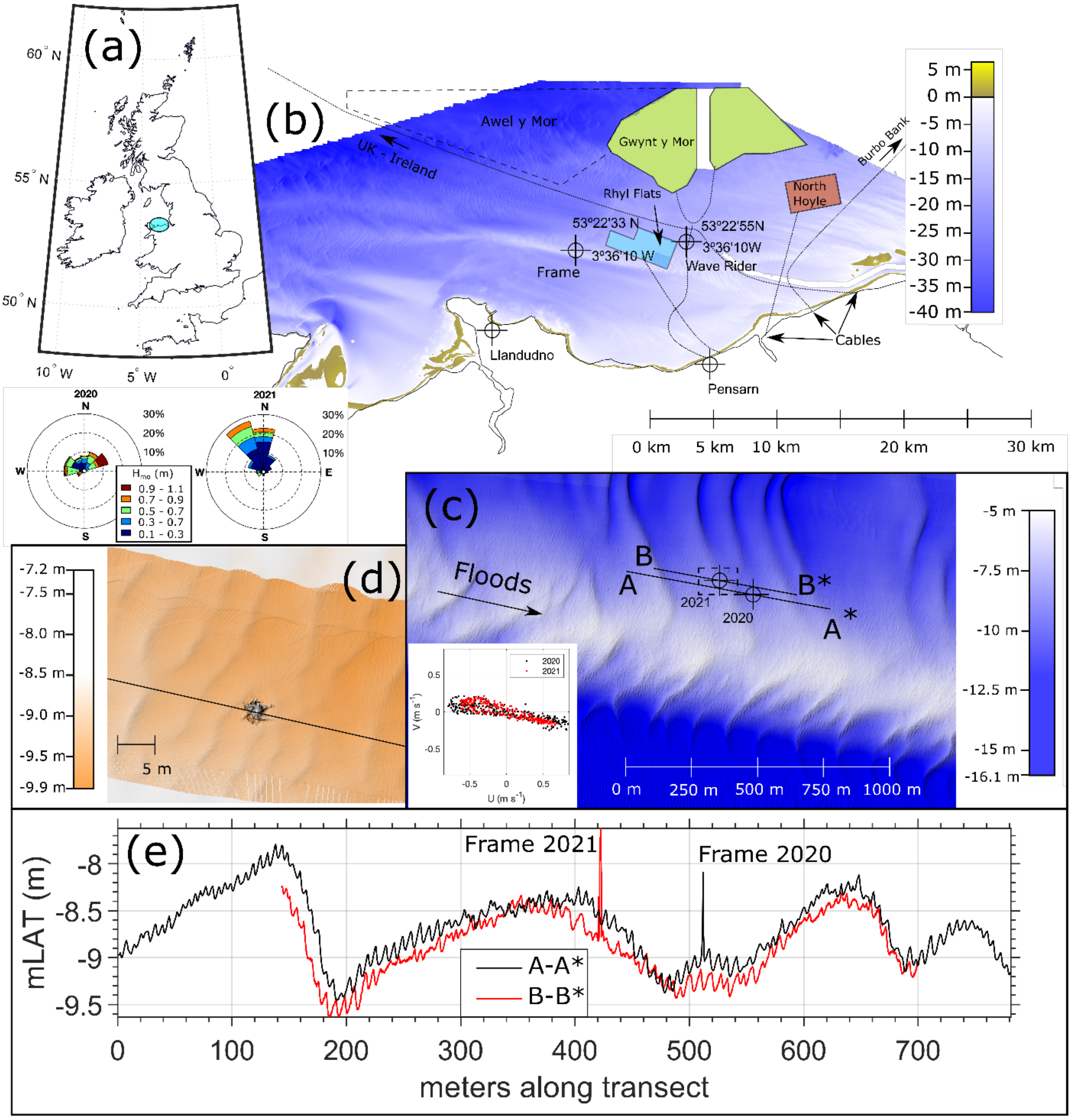

Figure 2. (a) Geographic projection of the UK and Ireland, with the location of the site of interest in light blue, with an inset of the wave roses for each deployment. (b) North Wales coastline and 2 m resolution bathymetry with existing wind farms in coloured polygons and proposed wind farms in dashed. Electric cables are indicated with dotted lines, (c) close up of Constable bank, with the transects A and B shown – these lines are also parallel to the mean flood tide direction at the site (inset shows measured tide directions), lander deployment locations and the outline of (d) shown with dashes.(d) close up of the deployment lander in 2021 with a 0.1 m resolution MBES line (orange to white) measured during the deployment, (e) Transects showing multiple bedform scales and the lander locations. 2020 MBES data, collected on 23/09/2020, 2021 MBES data collected on 15/07/2021

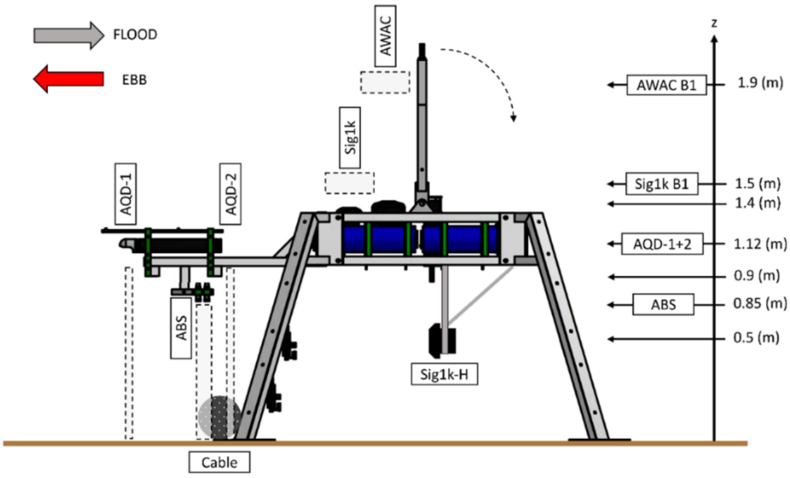

Figure 3. Schematic of the instrument lander and the location of instrumentation fixed to the lander. Dashed outlines indicate location of measurements used in the survey, "B1" indicates the location of the first bin of data. The section of cable is fixed to the base of the left side of the lander. Upon deployment, the arm at top of the lander swings down to the right upon release of the crane hook and the Sig1k and AWAC results are not affected by this arm. The Sig1k-H results are not used in the current paper.

2.2 Data Processing

The 600 kHz Nortek AWAC was deployed to quantify mean wave and current conditions during the surveys (Table 1, Figure 3). The data were processed by the onboard Prolog unit to derive the integrated directional spectral wave characteristics via the acoustic surface tracking method. This method also provides the near-surface current speeds. A small compass heading offset adjustment was performed in post-processing using information from the more accurate motion reference unit in the Signature1000.

The lander mounted an array of acoustic devices for measuring currents and suspended sediment concentrations, diagrammed in Figure 3. The Nortek Signature and Aquadopps were set to record in beam coordinates so that beam-based methods of estimating Turbulent Kinetic Energy (TKE) and Reynolds stresses could be used to then estimate turbulence production and dissipation (Guerra & Thomson, 2017; Rippeth et al., 2002). The combination of upward and downward facing ADCP's allows for the mean and near bed flow structure to be measured, including any effects from the bedforms on the flow field as well as the effects of the cable and instrument lander on the ebb tide velocities, especially near the bed. Standard thresholds for correlation and amplitude were set for ADCP's, which removed < 5% of data, velocity spikes were filtered out using a gradient threshold of 0.14 m s^{-2}. Removed values were replaced with linearly interpolated values, if the gap between good values was smaller than 4 data points. Velocities were converted to XYZ (Cartesian coordinates) and ENU (East, North and Up coordinates) in post processing. Rotation to a local three-velocity component (UVW) coordinate system was performed using the median flood tide direction for each instrument, so that $\overline{U}$ is maximised and $\overline{V}$ over time is minimised, and underwent a Reynolds decomposition into burst-mean (with overbar) and turbulent components (with prime) commensurate to our tidally dominated site

$$\boldsymbol{U} = (\overline{\boldsymbol{U}} + \boldsymbol{u}')[\boldsymbol{v}; \boldsymbol{w}]. \qquad \text{Eq. 3}$$

Bed shear stress $\boldsymbol{\tau_b}$ was calculated from the turbulent velocity components following (Soulsby & Dyer, 1981):

$$\boldsymbol{TKE = 0.5\rho(\overline{u'^2} + \overline{v'^2} + \overline{w'^2})} \qquad \text{Eq. 4}$$

$$\boldsymbol{\tau_b = 0.19TKE} \qquad \text{Eq. 5}$$

This has been shown to be the most accurate and reliable method of estimating bed shear stress in complex flows with localised point sources of shear and strong lateral gradients (Biron et al., 2004; Kim et al., 2000; Pope et al., 2006; Williams et al., 1999).

The Aquatec Aquascat Acoustic Backscatter System (ABS) was also deployed in downward facing orientation with 4 transducers to allow for the coincident measurement of flow and suspended sediment profiles. Scattering characteristic of the suspended sediments was estimated using the measured grain size distribution of the sediments with the method of Thorne & Meral (2008). Due to interference from the Aquadopp with the 1 and 2 MHz frequencies of the ABS, a multifrequency approach wasn't possible – so the ensemble average method of inverting the ABS backscatter was employed (c.f. Thorne and Hanes, 2002) with good agreement (within 10% concentration) between the higher frequencies which are not affected from the noise from the Aquadopp instrument.

Seabed bathymetry data were collected using a hull mounted Reson SeaBat T50 echosounder, using the highest frequency in the available range (400 kHz). Tidal corrections and corrections for the pitch and roll movements of the vessel were applied while processing the datasets using the Teledyne PDS 2000 software. The processed gridded data have a grid cell size between 5 cm and 20 cm.

Bed sediments are a fine sand with a D_{50} of 243 µm in 2020 and 245 µm in 2021, with D_{90}'s of 293 µm and 279 µm for both years. Thresholds of motion ($\boldsymbol{\theta}^*_{crit}$) and suspension ($\boldsymbol{\theta}^*_{sus}$) were calculated via the modified Shields curve (Soulsby, 1997):

$$\boldsymbol{D^* = D_{50}\left(\frac{(S-1)g}{v^2}\right)^{1/3}} \qquad \text{Eq. 6}$$

$$\boldsymbol{\theta^*_{crit} = \frac{0.3}{1+1.2D^*} + 0.055\,\{1 - exp(0.02D^*)\}} \qquad \text{Eq. 7}$$

where g is the acceleration due to gravity, ν is the kinematic viscosity of the sea water (at 15°C, 1.1384 x10^{-6} m^2 s^{-1} and s = 2.58 for quartz grains in seawater. The threshold for suspension is defined via (cf. van Rijn, 1993; Soulsby, 1997):

$$\boldsymbol{\theta^*_{sus} = \frac{0.3}{1+D^*} + -0.1\{1 - exp(-0.05D^*)\}} \qquad \text{Eq. 8}$$

At winter temperatures of 5 ºC, θ^*_{crit} for the sediments is 0.05 (0.2 N m^{-2}), and θ^*_{sus} 0.074 is (0.29 N m^{-2}). At typical summer temperatures of 15 ºC, θ^*_{crit} is 0.044 (0.18 N m^{-2}), and θ^*_{sus} 0.07 (0.27 N m^{-2}), indicating that seasonal variations in temperature account for a 12% difference in sediment mobility; the small difference in D_{50} between surveys produced a difference of <0.1%.

3.1 Results: Morphology of the seabed and water column during deployments.

The seabed bathymetry data at Constable Bank consists of sedimentary bedforms of two main scales. The larger scale bedforms in and around the lander site have an average length of 194 m by 0.94 m high (range from 0.8 – 1.5 m high, 200 – 300 m long), and have an orientation of 150° (Figure 3). Superimposed on these larger bedforms are smaller dunes of a scale 19 m long and 0.16 m high with a dominant angle of 100°, which is in line with the dominant flood tide direction. The location of the smaller bedform crests changed less than 0.1 m between the surveys in 2020 and 2021. Their shape changed during the tides in a similar way to estuarine bedforms (Lefebvre et al., 2022) where the location of the crest changed with tidal reversals, but the troughs did not. The size, shape and orientation of these smaller bedforms indicates there would be no/ or little significant flow separation from the larger host bedforms (Herbert et al., 2015). The height of the larger bedforms is roughly equal to the height of the instrument frame (1.4 m) so near bed flows measured by the lander are within the turbulent boundary layer generated from the bedforms (Dyer, 1986; McLean et al., 1999; Nowell & Church, 1979).

The September 2020 deployment occurred during the autumnal equinox, producing some of the largest tides of that year. The deployment began during spring tides with water depths ranging between 9 – 17 m and associated high mean velocities of 0.75 – 1 m s^{-1} (Figure 4a, c). Conditions transitioned to neap tides at the end of the survey with water depths of 10 – 16 m and velocities in the range 0.85 – 0.6 m s^{-1}. The 2021 survey was during a smaller spring neap cycle, 10 – 16 m water depth, with velocities peaking at 0.7 and reducing to about 0.5 m s^{-1} (Figure 4b,d); the tidal ranges surveyed are typical of peak (2020) and average (2021) annual tidal forcing.

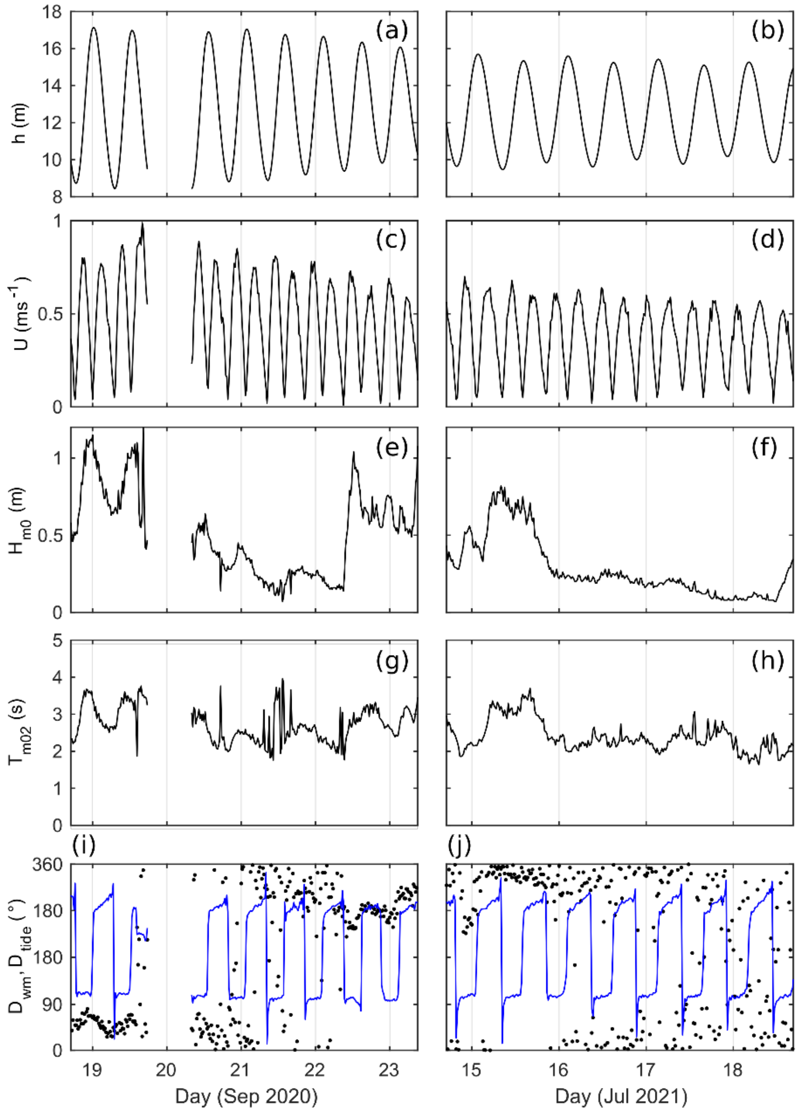

Figure 4. Hydrodynamic forcing recorded by the AWAC during the field observations, September 2020 left panels, July 2021 right panels. (a, b) Water depth h; (c, d) mean near-surface tidal current speed U; (e, f) significant wave height H_{m0}; (g, h) mean wave period T_{m02}; and (i, j) mean wave direction D_{wm} (black dots) and tidal directions (blue line). All directions are from North.

Wave activity peaked during the start of the 2020 survey with H_{m0} = 1 m and T_{m02} = 3.5 s (Figure 4e, g), reducing to H_{m0} < 0.5 m, before again peaking towards the end of the survey with H_{m0} = 0.6 – 1 m. Long term (2007 – 2021) wave buoy data from the Rhyl Flats wave rider shows that 1 m high waves have an exceedance of 80%, indicating that these waves are relatively common in any given year. The 2021 surveys were mostly very calm with H_{m0} < 0.4 m, except across the first two tidal cycles at the start of the survey where H_{m0} = 0.7 m and T_{m02} = 3.5 s (Figure 4f, h). Flood tide direction was a consistent 100° (Figure 4i, j), whilst ebb tides show a rotation between 320° to 270°, typical of the flood dominant tidal conditions in the bay. Wave directions were rarely aligned with the tides during the surveys, with the main wave events arriving from a more northerly direction, suggesting the net bed shear stress direction under combined flows will be deflected southwards. The hydrodynamics during the surveys were therefore typical of average to peak tidal forcing conditions, with average to calm wave conditions.

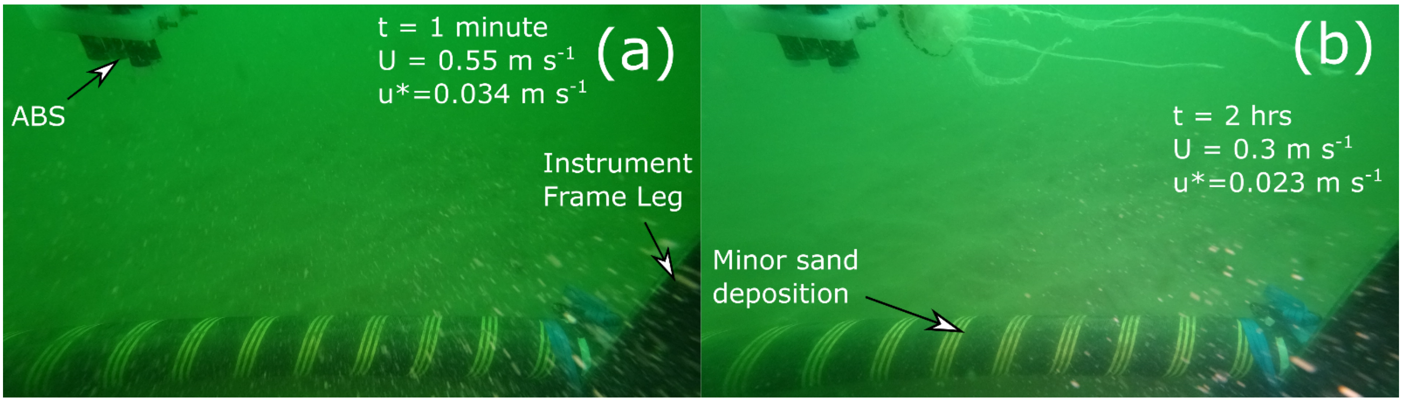

Figure 5. Photographs from a lander-mounted time lapse camera, with lamp positioned to the right of the image, on 14/07/2021. (a) The first image of the lander on the seabed, the cable, part of the instrument lander leg, and the ABS can be seen. After two hours (b) a small amount of sand can be seen resting on the cable, at this point no other deposition or scour is observed. A video of the photographs is provided in the supplementary material.

A time lapse camera and light were mounted on the lander for the 2021 survey, to monitor the seabed and any depositional changes around the cable. Whilst the battery was drained after only 4 hours, Figure 5 illustrates that the images do provide some useful context. For the initial ebb to flood measured by the camera, no obvious scour was evident around the cable from the pictures taken. A small amount of sediment appeared on top of the cable after the initial settling of the lander on the bed, suggesting that there is flow separation occurring on the lee side of the cable with a flow speed of about 0.27 m s^{-1} (measured from AQD-1). The rippled sand bed visible in the background did not appear to move at all during the 4 hours of footage taken, with a near bed flow speed up to 0.3 m s^{-1}; this lack of sediment motion combined with the lack of any scour from the cable or lander feet suggests the sediments were largely immobile upon deployment in 2021.

3.2 Results: Bed levels and cable burial

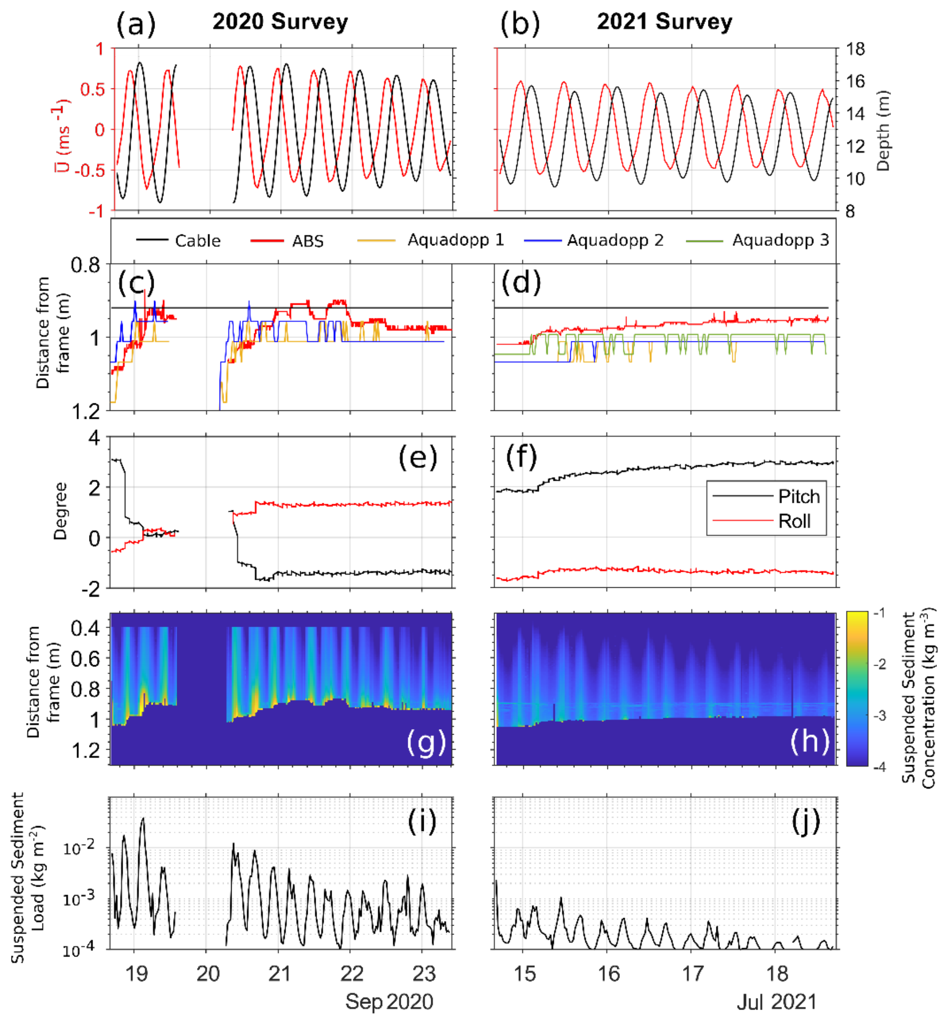

Figure 6. (a & b) Burst average current speeds (red) and flow depths (black) from the upward facing Nortek Signature, with (c & d) downward facing acoustic instruments' measure of the bed level, relative to the top of the cable. (e & f) show the pitch and roll as measured by the upward facing signature (centrally positioned in the lander) from both deployments. (g & h) suspended sediment concentrations in log10 colour scale, with suspended sediment loads (integrations of the profiles) shown in (i & j).

Depth-averaged mean velocities as measured by the upward facing Nortek Signature (Figure 6a-b) are lower than the current speeds shown from the AWAC in Figure 4c-d, due to the AWAC data being a near surface current speed rather than the depth-averaged. Peak depth-average mean current speeds in 2020 are around 0.6 m s^{-1}, and 0.5 m s^{-1} in 2021, and the phase lead of the velocity with respect to the water depth due to the standing tidal wave results in peak flows occurring during mid-flood and mid-ebb. The 2020 survey's two deployments can be seen either side of the gap in data around September 20th. For both deployments in 2020 the bed appears to rise by 0.2 m during the first two tides of each deployment (Figure 6c). Gyroscope data from the instruments (Figure 6e-f) suggests that the rear (ebb facing) side of the lander sank slightly during the first tide of both deployments in 2020. After one tide both deployments in 2020 show a stable pitch and roll. The change in lander angle is only enough (at most) to change the distance to the bed as measured by the ABS by 0.0024 m, indicating that the changes in bed elevation during this time are not due to the angle of the instruments changing. It is possible that if there is erosion around the legs of the lander this could be a source of sediment for deposition around the cable. The 2021 survey by comparison shows a gradual one-degree drift in pitch and roll during the survey. Although we cannot know for certain, it seems likely that the cable attached to the flood facing side of the lander actually prevented the lander from sinking at that end. The elevation of the cable (as measured by the ABS) during the deployments did not appear to change suggesting that the cable did not experience underscour and settlement. The change in pitch over time in 2021 has a similar trend to that of the bed level measured by the ABS, but a change in angle of 1° for a profile 1 m long would be nearly impossible to detect even with the ABS bin resolution of 0.5 cm. The simultaneous change in pitch and bed level is suggestive of the rear of the lander sinking slightly, which may be suspending some of the sediment which was measured in the surveys.

The higher resolution and more precise data of bed levels from of the ABS show that the bed reached the height of the cable during two ebb tides between September 21st and 22nd (Figure 6c) – which was after the lander had stopped shifting. After these two tides, bed levels appear to stabilise at around 1 m away from the lander. The 2021 survey does not show a similar rapid response in bed level to the presence of the cable and instrument lander: with gradual deposition settling measurable during the deployment (Figure 6d), up to 20 cm by the end of the survey.

Suspended sediment concentrations during the two deployments of the 2020 survey exceed $O(10^{-2})$ kg m^{-3} in the first two tides. This coincided with deposition of 0.2 m during both deployments indicating a consistent sequence of suspended sediment load and bed level change. The less energetic 2021 survey showed lower suspended sediment loads of $O(10^{-3} - 10^{-4})$ kg^{-1} m^{-3} (Figure 6j), with little sediment suspended higher than 0.5 m above the seabed (Figure 6h); conversely the 2020 survey showed clear flood and ebb suspensions in the entire ABS profile (Figure 6g). The larger suspended sediment concentrations, and changes in the seabed at the start of the deployments suggests that these higher concentrations are more likely to be during a period of higher sediment mobility.

There is no obvious reason for the distinct difference in seabed response and sediment suspension between the 2020 and 2021 surveys. The seabed sediment particle size analyses did not identify any disparity between surveys which would account for a change in mobility of this magnitude. The position of the lander in the bedform field (Figure 2) was on the lee side of a large bedform in 2021, and in a trough in 2020, therefore we would expect to see similar mobility affects from the known spatial variation of sediment mobility over marine dunes (Damveld et al., 2018). It is possible that the 2021 position is more sheltered to the flood tides, but this is not apparent in the mean velocity, nor near bed turbulence data measured form the lander. The most comparable tidal ranges between surveys are the largest tides in the 2021 survey and the end of the 2020 survey, and comparing these tides shows there was nearly an order of magnitude difference in suspended sediment loads for these similar tides. It is also notable that the distance to the bed first measured upon deployment, and the amount of movement of the lander were both greater in 2020 than 2021, suggesting the seabed was more cohesive and/or stronger in 2021, than 2020. This difference in overall mobility also appears to have affected how much and how quickly the self-burial processes occurred over the surveys. The next section investigates how burial of the cable itself by sediment accretion has affected the hydrodynamics over the cable which contribute to the self-burial.

3.3. Effects of cable burial on flow and turbulence

The presence of the lander and cable, moderated by the variation in bed level, should have impacted the form of the near bed turbulence and velocity profiles, with 2020 data less impacted than in 2021 due to greater burial of the cable in 2020. Figure 7 assesses the shape of the mean velocity, turbulent kinetic energy profiles and suspended sediment concentrations over peak flood and ebb current speed of a tide for both lander deployments. Clear differences in the form of the mean velocity profiles for equivalent times during flood and ebb are evident (Figure 7a, b). The flood conforms to the expected theoretical logarithmic form, whereas the ebb departs from this form becoming depth-invariant and even decreasing above y = 0.6 m. For the 2021 comparison (Figure 7b) with a greater cable exposure, the flow is faster above the cable, and slower below the cable height. The TKE profiles (Figure 7c, d) approximately follow the expected form during flood tides. During the ebbs the impact of the cable and lander higher in the water column are evident with high TKE values near and below the height of the cable between 0.8 and 1 m. For the more exposed cable 2021 data – near bed TKE is 50% higher compared to the mid profile.

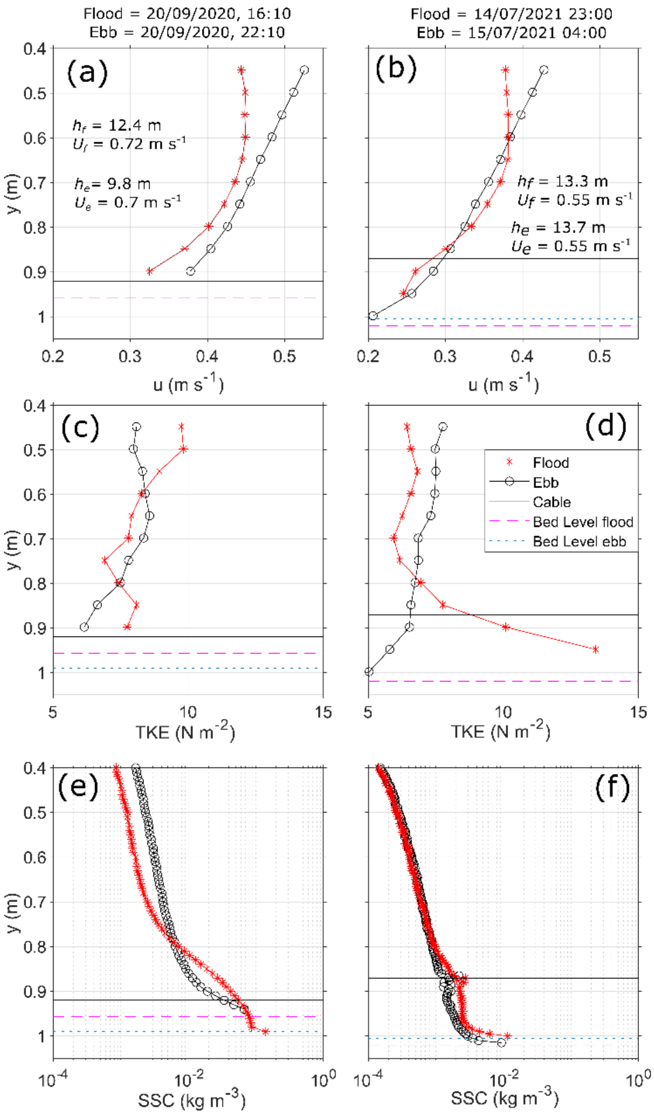

Figure 7. Flood (black) and ebb (red) profiles of mean velocity (a, b), turbulent kinetic energy (c, d), and suspended sediment concentration (e, f), for the September 2020 (left) and July 2021 (right) deployments. Distances on the y axis are range from the Aquadopps 1 & 2 mounting elevation and indicate the top of the cable. The bed level changes between profiles in 2020 but is constant for the two profiles in the 2021 plots. Time the profiles were measured, and the depth averaged mean velocity from the upward facing Signature 1000 are given as reference at the top of the figure.

Suspended sediment profiles in the 2020 survey demonstrate greater near bed suspension in the ebb tides compared to flood – in spite of the background suspended sediment concentration (indicated by SSC higher in the profile) being lower for ebb than flood. This indicates that the enhanced turbulence from the presence of the lander and cable is also enhancing suspended sediment concentrations. The 2021 survey, however, shows very little difference in profile shapes (Figure 7b), and overall lower concentrations (Figure 7f) – which are nearly equal in flood and ebb. TKE is similar or higher than the 2020 profiles indicating that the presence of the cable and lander is producing greater near bed turbulence in 2021 than 2020 (Figure 7c-d), this enhanced (relative to flood tides) turbulence seems to have also increased the suspended sediment concentrations at the bed and near the cable, while concentration closer to the lander (y=0.4) are equal in floods and ebbs (Figure 7f).

It is clear that the two deployments show differing effects of the extra drag from the cable and instrument lander. The 2020 suspended sediment profiles are more greatly affected than 2021, yet the 2021 flow data are more obviously affected by the cable – likely due to the higher exposure of the cable above the seabed in the 2021 survey, whereas the 2020 survey showed evidence of cable burial due to sediment deposition (Figure 8). This is further suggestive of a change in sediment mobility between surveys, and if so, suggests that overall bed sediment mobility affects cable burial processes more than the direct effects of turbulence generated by the cable itself.

3.4. Timing of burial and bed shear stress

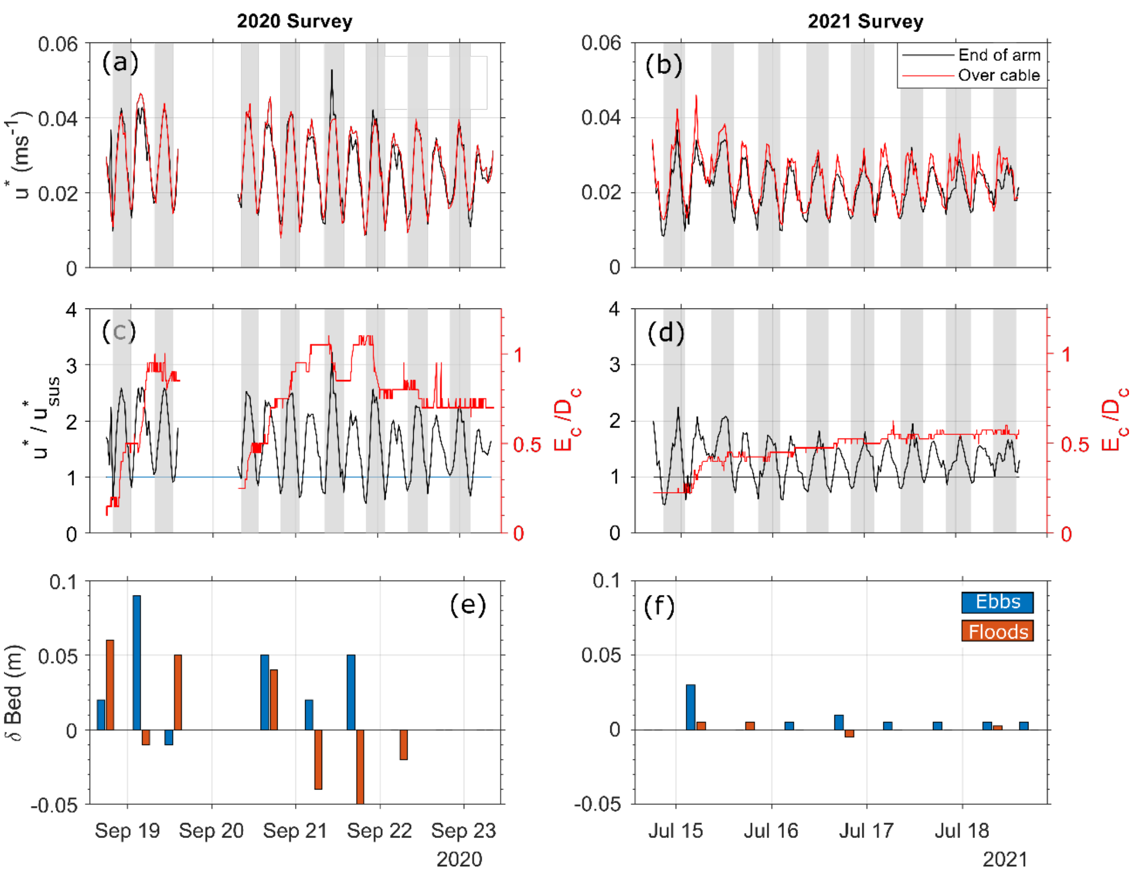

Figure 8. (a,b) u* derived from the TKE method of estimating bed shear stress for both Aquadopps. Estimates from over the cable (AQD-2) are often higher in ebbs compared to the instrument at the end of the frames arm (AQD-1). Shaded areas indicate flood tides. (c&d), bed levels plotted with u* from the over the cable Aquadopp scaled by the initiation of suspension for the bed sediments, (e&f) change in the embedment of the cable over individual flood and ebb tides, positive values indicate deposition, negative is erosion.

The two Aquadopps on the lander arm (Figure 3, AQD-1 and AQD-2) let us quantify the amount of shear coming directly from the cable and if the effects of cable burial modified it. Figure 8a-b show the estimate of the shear velocity (which drives sediment transport) derived from the TKE (equations 4-5). The values for u* from both Aquadopps during the flood tide are nearly identical whist during ebbs u* measured over the cable (AQD-2) is often (but not consistently) higher than that measured at the end of the lander arm (AQD-1). Ebb tides in the 2020 deployment in Figure 8a, b show higher TKE derived u* from the Aquadopp over the cable in the first tides from all deployments by 20 – 30%, and 10 – 15 % higher thereafter at peak ebb tide. In 2021, where there is less change in the bed elevation, there also is no obvious change in the flood/ebb asymmetry of peak u*, further indicating that any morphological changes around the lander and cable were not altering the hydrodynamics much for this survey.

Normalising the shear velocity ($u* = ({}^{\tau_b}/_{\rho})^{0.5}$ with $\boldsymbol{\tau_b}$ from Eq.5) by the threshold of suspension in $u*$ form (from Eq. 6-8) shows that 84% of all measurements are above the threshold of suspension (Figure 8c-d). As the diameter of the cable is known, the height of the seabed next to the cable, and the height of the cable itself above the seabed are measured by the ABS (within 10 cm of the cable), a direct measure of the embedment depth (E_c) can be produced. $E_c$is plotted in red on (Figure 8c-d) and shows that much of the change in bed level is happening near peak bed shear stress of each tide. Figure 8g-h quantifies the amount of deposition (or erosion) for each flood and ebb and demonstrates that aside from the first 1 – 2 tides of all deployments, if there is morphological change, flood tides erode whilst ebbs always deposit sediment. Such a process could either be movement of sediment from one side of the cable to the other over a tide, but as there are no measurements of bed level of fine enough resolution (AQD-2 does have 1 beam on the ebb side of the cable), we cannot confirm or reject that hypothesis. The constant increase in burial in 2021 indicates that although transport was weak during these tides, some form of self-burial process was slowly occurring. In 2020 it is clear that there was a rapid deposition of sediment on either flood or ebb tide during the first two tides, followed by erosion of the sediment around the cable on floods and deposition on ebbs – indicating a rapid partial burial of the cable – followed by a volume of sand migrating to either side of the cable on each phase of the tide. The next section discusses these observations and places the results into a wider context of previous work about self-burial processes and cable scour.

4. Interpretation and discussion.

Here we present the data from an offshore campaign where cable seabed interaction is monitored in real-time, quantifying mean flow, turbulence and suspended sediments. Whilst surveys of cables are commonplace, campaigns where laboratory style equipment and measurements are used to measure processes happening in high detail are rare, but provide insight into the interaction of cables and the seabed processes (Leckie et al., 2015, 2016, 2018), and biologically induced burial of pipelines (McLean et al., 2022; McLean et al., 2020), which produce new information and knowledge which can be used to improve cable and pipeline stability assessments. Whilst the spatial variability of seabed conditions is a key control on the potential for seabed mobilisation, and thus the burial process, the results we present here focus on the temporal variability in one location where the seabed is similar. Our study suggests that processes other than the typically used cable diameter, embedment depth and mean flow, control the burial process. In the section below we discussed these processes, and how they are enough to modify the rate and intensity of cable burial.

4.1 Scour vs deposition

For a deployment under relatively fast currents and a mobile sand bed, it was largely expected at the start of the surveys that scour would occur beneath the cable. Yet the observations during this study all indicate that no scour occurred, and that instead burial processes dominated. To confirm the observations of no scour under the central portion of the cable, the breakthrough for tunnel scour in granular sediment was evaluated using the formula fitted to laboratory experiments by Sumer & Fredsøe (2002). Values for the reference velocity at the top of the cable were taken from the ADCP bin closest to the cable from AQD-2 (as is required by the model), the results are shown in Figure 9a.This difference between deployments could be due to greater sheltering from the flood tides due to the position of the 2021 lander on a lee slope of a larger bedform (cf. Figure 2e) and suggests that cable positioning upon deployment could prefer bedform lee slopes to reduce U_{ref}^2, and lower the risk of scour.

Plotting U_{ref}^2 also demonstrates a large difference in velocity above the cable between deployments (Figure 9b & 9c), with the 2021 survey U_{ref}^2 about half that of the 2020 data, despite the neap tides in 2020 (when transport did occur) and spring tides in 2021 (with little observed transport) having similar tidal ranges. This difference in near bed flow speed between deployments could be due to greater sheltering from the flood tides due to the position of the 2021 lander on a lee slope of a larger bedform compared to the more exposed position in 2020 (cf. Figure 2e). Whilst the frame itself may have been in a more sheltered location in 2021, the greater exposure of the cable to the flow due to lower embedment depths did produce higher TKE around the cable than in 2020 (Figure 7c-d), suggesting that the effects of the cable on the near bed flow are still important even though U_{ref}^2 (and therefore risk of scour) was lower in 2021.

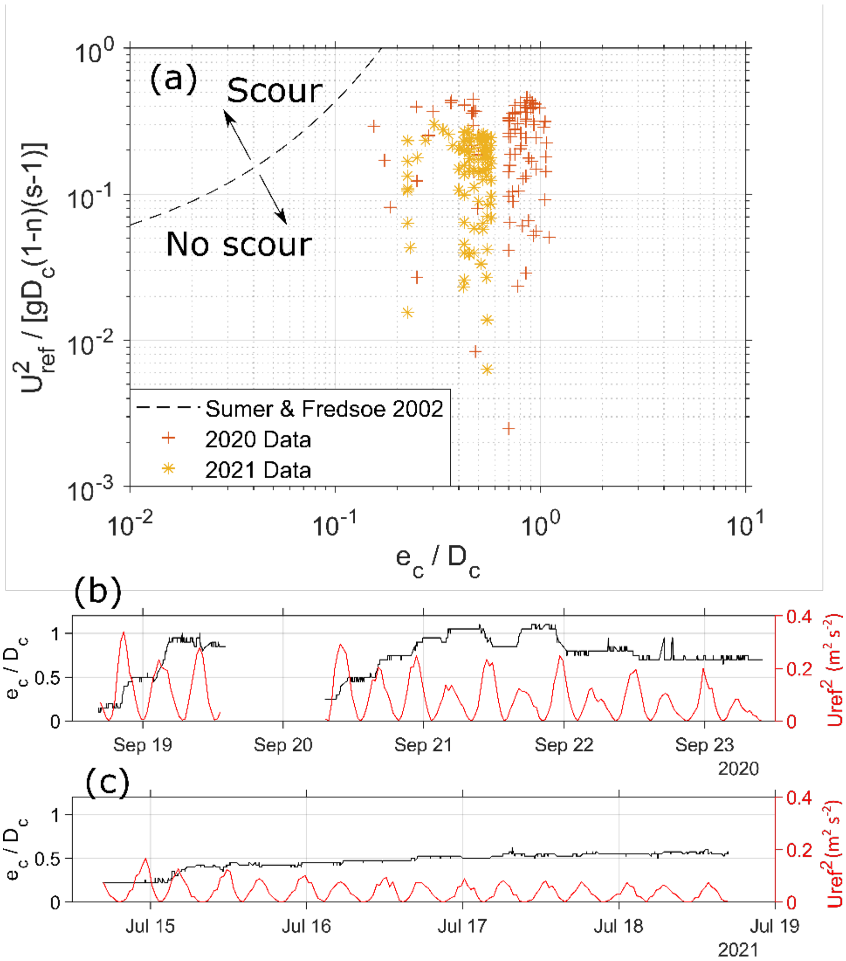

Figure 9. (a) Dashed line is the onset of scour under a rigid cable on the seabed **(**Equation 1; Sumer & Fredsøe, 2002) and the values measured in this study. (b) and (c) show the values in (a) plotted with time for the 2020 and 2021 deployments respectively.

4.2 Seabed Mobility

One of the surprising findings from the surveys was the differing responsiveness of the bed and the suspended sediment concentrations. To investigate this further, the suspended sediment loads (C) from each survey are plotted against $u*$ estimated (Figure 10) from the AQD-1 using the TKE method (Soulsby & Dyer, 1981). The empirical threshold of motion (in $u*$) of the sediments is 0.0134 m s^{-1} and is used to normalise the x axis. Whilst there is nearly an order of magnitude scatter in C per value of u^*/u_{sus}^*, there is a clear separation in the distribution of C between each year's data (Figure 10a). To illustrate how different the seabed mobility was between surveys, three different values for u_{sus}^* across a broad range {0.01 0.02 0.04} were applied to the 2021 data (Figure 9b). These thresholds of motion correspond to the grain sizes {45 900 2500} µm. An adjusted u_{thr}^* of 0.02 collapses the 2021 data onto the 2020 data and is equivalent to a sand grain diameter of 900 µm, four times larger than the D_{50} from both year's grab samples, but clearly not representative of the seabed sediments which were measured from the PSD of the grab sample.

With a direct estimate of the bed shear stress from near bed turbulence data applied and variation in grain size distribution minimal, we see very few reasons why there would be such a difference in seabed mobility, so in the following section we suggest several hypotheses which may explain the large difference in seabed mobility. A bimodal sediment mixture can alter the threshold of motion by the magnitude observed through the hiding-exposure effect (McCarron et al., 2019). The grab sample sediment sizes ≥ 900 µm made up < 0.1 % of the grain size distributions and are therefore too few to affect the mobility of the sediment via this process, and these distributions are reasonably similar between both years' grab samples. So, whilst this process does occur in the region, our data do not support it as a major factor at the survey site. Adding in a small amount of coarser sediment into the grain size distribution (whilst keeping it unimodal) has demonstrated a change to mobility in laboratory experiments (MacKenzie & Eaton, 2017). Such fine scale variability is not impossible in the environment we survey, but an introduction of new coarser sediment into the system seems unlikely given the location of the site and the grab samples obtained. The "armouring" process hypothesised by (MacKenzie & Eaton, 2017), is a possible candidate as an explanation for our results but little work has been conducted on the armouring of sand only sediments. Near bed sorting processes like this, and the variability in seabed mobility they produce, is often considered a form of "natural variability" in seabed sediment dynamics as it is often too difficult to measure. In fluvial environments, particularly coarse-grained rivers (Dietrich et al., 1989; Vericat et al., 2006), more work has been concluded on this topic due to the ease of measuring the active layer of sediment transport (Hassan et al., 2020; Pähtz et al., 2020), whilst subtidal work has often focused on broader changes of mobility due to fines (Amos et al., 1997; Thompson et al., 2011). We suggest that changes in the mobility of unimodal sands could be detectable in long term (> 1 month) long field surveys of seabed mobility where a drift in the relationship between bed shear stress and suspended sediment concentrations would occur over these timescales due to near bed sorting processes modifying the top layer of sediment.

Lastly, one other cause which can alter sediment mobility, which was not measure in these surveys, is the presence of extracellular polymeric substance (EPS) producing organisms. Recent work has illustrated that EPS can influence sediment mobility by an order of magnitude either from the EPS itself (Chen, et al., 2017a), or from the fines that EPS introduce into the bed (Chen, et al., 2017b; Hope et al., 2020). It is notable that the camera pictures on the 2021 frame (Figure 5) showed green seawater which should indicate the presence of plentiful marine microorganisms. Seafloor measurements of EPS are rare, with most measurements in intertidal and riverine environments where access is much easier (e.g., Chen, et al., 2017a,b; Hope et al., 2020; Paterson, 1989; Underwood & Paterson, 1993). Furthermore, recent intertidal surveys have shown that even small (1 – 2 % by mass) quantities of mud and/or clay can alter bed mobility by 2 – 3x (Hope et al., 2020; Lichtman et al., 2018), so a similar scale of the changes in mobility found in the current study. Further work is needed to confidently state if EPS, mud and clay content are components of the sea floor system which are moderating the in-seabed mobility seen in the present study. From our own samples, sediment sizes < 63 μm made up < 1 % of the grab sample (by mass) but as the sampling strategy was designed for sand and coarser sizes, clay, mud and silt could have been lost in the process. Visual surveys of sub-tidal dune beds have also shown high spatial variability in grain size, mud and possible biological effects on the seabed (Damveld, et al., 2018). It seems plausible that our grab samples could have missed, by chance, this small-scale variability. As such we encourage a spatial visual and grab sample survey to be sure of ground conditions upon deployment, when subtidal bedforms are present.

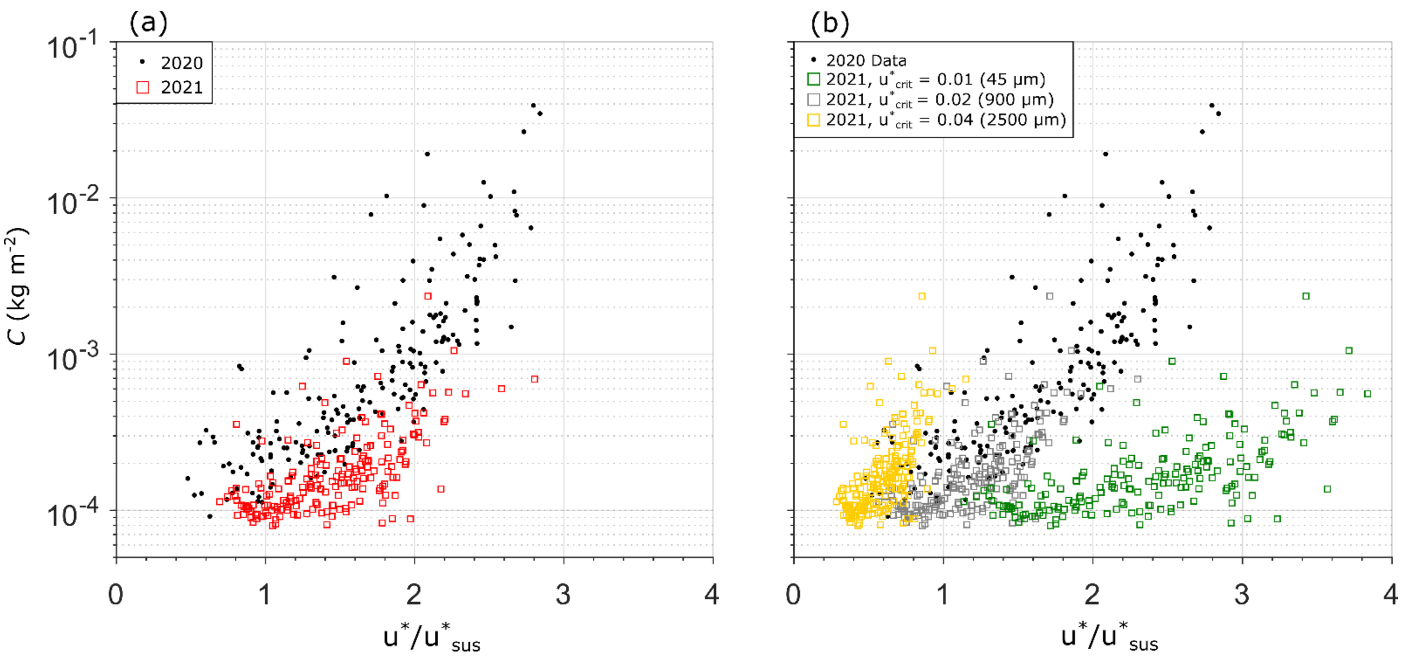

Figure 9. (a) Scatter plot of burst average suspended sediment load (*C*, kg m^{-2}) versus the normalised shear velocity for each burst, with a value of 0.0134 m s^{-1} for u^*_{sus} estimated from eq.6-7. Panel (b) shows the same *C*, but as a sensitivity check for the 2021 data three different values for u^*_{sus} (equivalent grain size at 10°C are given in parenthesis) were used to normalise u^*.

4.3 Turbulence modification and self-burial

The present surveys allow us to directly investigate the amplification of shear using AQD-2 directly above the cable and compare it to the ambient shear stress recorded by AQD-1. Figure 11 shows the ratio of the peak tidal (for floods and ebbs) shear velocity from these two Aquadopps, plotted with the embedment ratio. Here we see that in the 2020 survey, as the embedment ratio increased to well over 50%, the ratio of peak shear stresses reduces and even becomes < 1, indicating that at higher embedment (near unity) the turbulence near the cable is actually lower than in the free stream. The 2021 survey is more inconclusive, embedment reaches >50%, but the ratio of peak stresses is not cleared altered in response – turbulence near the cable clearly remains amplified during both floods and ebbs. This comparison suggests embedment depths much greater than 50% are needed to noticeably reduce turbulence over a cable in this kind of environment.

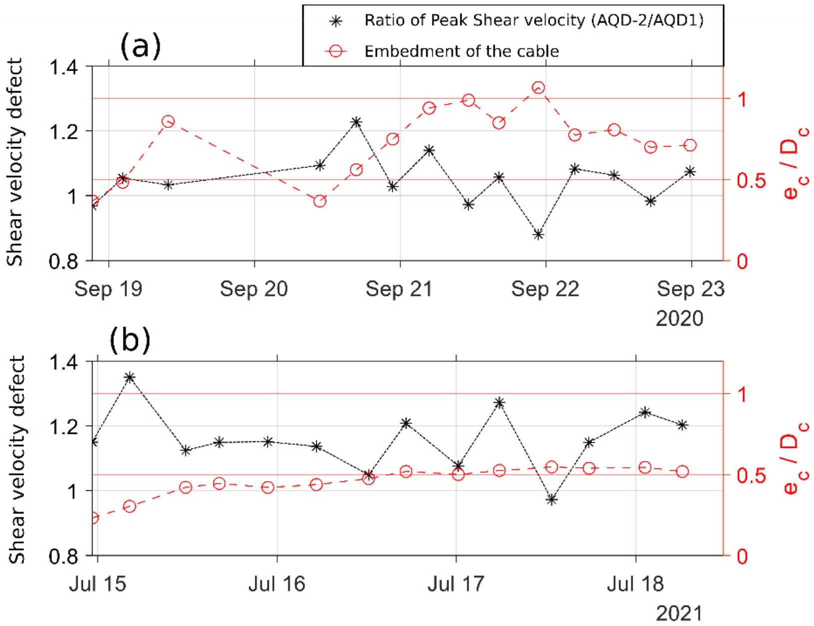

Figure 11. the ratio of peak shear velocity (AQDP-2 over cable / AQDP-1 end of arm) per flood and ebb, with the embedment of the cable shown on the right axis, for 2020 (a) and 2021 (b) surveys. Values on the left y axis > 1 show higher $u*$ occurred during ebb tides.

Previous research has found that for embedment depths of 50% or greater, the reverse flow in the lee wake (Figure 1) moved sediment towards a pipeline (Chiew, 1990). From our surveys, this kind of self-reinforcing process appears to occur for all conditions regardless of the embedment depth – notably in 2021 where gradual deposition around the cable was observed with a starting embedment depth of 20%. So, we suggest that under the conditions observed during our surveys, cables Zhao et al. (2015) showed a net influx of sediment in the volume around a pipeline was a large contributing factor to sedimentation, and the beginning of the 2020 survey seems to support this concept on a real in-field example, with suspended sediment loads up to 0.04 kg m^{-3}, and as concentration dropped during the survey flood tides started to erode rather than deposition sediment.

Our repeated multibeam surveys in 2021 showed no measurable sediment build up around the lander and sediment suspension, even with the enhanced turbulence produced by the cable. The results in Figure 11 confirm that for embedment by sediment build-up of up to around 50% the local shear velocity is enhanced by 15 to 20%, and with the streamlining effect of 75-100% embedment value of local shear stress is about the same as the ambient. It appears that for the 2021 conditions at the site, an increase in peak shear stress at the cable location of nearly 40% above ambient level was insufficient to mobilise much sediment, even though nearly all the measurements were above the threshold of motion and suspension as calculated from standard equations (*Eq.4-6*). This combination of factors strongly suggests that an unmeasured differential seabed mobility between 2020 and 2021 was affecting the relationship between bed shear stress and suspended sediment concentration, and subsequently the process of cable burial, and that future work is required to fulling understand what controls mobility – even when the sediments are uniform and well sorted, with < 1 % fines or coarse fractions.

5. Conclusions

Field surveys conducted in a region of existing and expanding offshore renewable energy infrastructure quantified the mean flow, turbulence, sediment suspension and bed levels around a section of typical subsea electricity cable. The survey results found that the initial embedment depth of the cable and the flow conditions above the cable upon deployment were good indications of the trajectory of the bed response. The bedform field at the site indicated that there was sediment mobility and hence at the start of all deployments as the cable was placed in contact with the bed scour under the cable should theoretically have occurred due to tidal flow, yet self-burial processes through sedimentation existed through the surveys. This could be due to the embedment depth of the cable increasing upon deployment, as in our surveys in 2020. However, subsequent surveys in 2021 indicated a self-burial process occurred with little sediment in suspension and despite enhanced turbulence originating from the cable.

Despite the location of both deployments being similar, there was a large difference in the seabed response and the suspended sediment concentrations between the two surveys, and there is no clear answer to why. It is suggested that the larger tides and typical wave conditions at the start of the 2020 survey produced a more mobile seabed compared to the calmer (but not atypical) conditions during which the 2021 survey occurred. Paradoxically, the 2021 survey's lack of sediment suspension and seabed changes lead to a more exposed cable and an enhancement of 30 – 40% more turbulence produced by the cable compared to ambient flow. However, this enhanced turbulence did not seem to affect sediment suspension or cable burial, despite peak bed shear stresses being twice the initiation of motion or suspension for the sediments. In the more mobile 2020 surveys, cable burial reduced the excess turbulence produced by the cable to an immeasurable difference to the ambient condition as embedment depth tended to unity. Once this state was reached the seabed around the cable varied on each phase of the tide. For all surveys, deposition occurred around the cable – but at very different rates dependent on forcing and local bed conditions. The turbulence induced from the cable itself appeared to lead to locally increased sedimentation around the cable.

6. Acknowledgements

This work was funded by the ESPRC Supergen ORE Flexible Fund grant FF2020-1095 and the ECOWind-ACCELERATE project (NE/X008886/1) Project. Additional support was provided by the Smart Efficient Energy Centre (SEEC) funded by the Welsh European Funding Office (WEFO) as part of the European Regional Development Fund (ERDF). AJC and RJSW also acknowledge provision of matching funds from the HR Wallingford strategic Scour Research Programme. The team thanks Ben Powell, Aled Owen, and the crew of the RV Prince Madog for facilitating this fieldwork under difficult working conditions due to COVID-19 restrictions.

7. References

Amos, C. L., Feeney, T., Sutherland, T. F., & Luternauer, J. L. (1997). *The Stability of Fine-grained Sediments from the Fraser River Delta*. *Estuarine, Coastal and Shelf Science* (Vol. 45).

Bennett, S. J., & Best, J. L. (1995). Mean flow and turbulence structure over fixed, two-dimensional dunes : implications for sediment transport and bedform stability. *Sedimentology*, *42*, 491–513.

Biron, P. M., Robson, C., Lapointe, M. F., & Gaskin, S. J. (2004). Comparing different methods of bed shear stress estimates in simple and complex flow fields. *Earth Surface Processes and Landforms*, *29*(11), 1403–1415. https://doi.org/10.1002/esp.1111

Chen, X. D., Zhang, C. K., Paterson, D. M., Thompson, C. E. L., Townend, I. H., Gong, Z., Zhou, Z, Feng, Q. (2017a). Hindered erosion: The biological mediation of noncohesive sediment behaviour. *Water Resources Research*, *53*(6), 4787–4801. https://doi.org/10.1002/2016WR020105

Chen, X. D., Zhang, C. K., Zhou, Z., Gong, Z., Zhou, J. J., Tao, J. F., Paterson, D. M., Feng, Q. (2017b). Stabilizing Effects of Bacterial Biofilms: EPS Penetration and Redistribution of Bed Stability Down the Sediment Profile. *Journal of Geophysical Research: Biogeosciences*, *122*(12), 3113–3125. https://doi.org/10.1002/2017JG004050

Chiew, B. Y. (1990). Mechanics of Local Scour Around Submarine Pipelines, *Journal of Hydraulic Engineering*, 4 (515), pp. 515-529, 10.1061/(ASCE)0733–429(1990)116

Couldrey, A. J., Benson, T., Knaapen, M. A. F., Marten, K. V., & Whitehouse, R. J. S. (2020). Morphological evolution of a barchan dune migrating past an offshore wind farm foundation. *Earth Surface Processes and Landforms*, *45*(12), 2884–2896. https://doi.org/10.1002/esp.4937

Damgaard, M., Andersen, L. v., & Ibsen, L. B. (2015). Dynamic response sensitivity of an offshore wind turbine for varying subsoil conditions. *Ocean Engineering*, *101*, 227–234. https://doi.org/10.1016/j.oceaneng.2015.04.039

Damveld, J. H., van der Reijden, K. J., Cheng, C., Koop, L., Haaksma, L. R., Walsh, C. A. J., et al. (2018). Video Transects Reveal That Tidal Sand Waves Affect the Spatial Distribution of Benthic Organisms and Sand Ripples. *Geophysical Research Letters*, *45*(21), 11,837-11,846. https://doi.org/10.1029/2018GL079858

Dey, S., Paul, P., & Padhi, E. (2020). Conditional spatially averaged turbulence and dispersion characteristics in flow over two-dimensional dunes. *Physics of Fluids*, *32*(6). https://doi.org/10.1063/5.0008380

Dietrich, W. E., Kirchner, J. W., Ikeda, H., & Iseya, F. (1989). Sediment supply and the development of the coarse surface layer in gravel-bedded rivers. *Nature*, *340*(6230), 215–217. https://doi.org/10.1038/340215a0

Dyer, K. R. (1986). *Coastal and estuarine sediment dynamics*. Chichester, U. K.: John Wiley & Sons.

El Mountassir O, Strang-Moran C. Offshore Wind Subsea Power Cables. Installation, Operation and Market Trends. *University of Hull*; 2018.

Guerra, M., & Thomson, J. (2017). Turbulence measurements from five-beam acoustic doppler current profilers. *Journal of Atmospheric and Oceanic Technology*, 34(6), 1267–1284. https://doi.org/10.1175/JTECH-D-16-0148.1

Hassan, M. A., Saletti, M., Johnson, J. P. L., Ferrer-Boix, C., Venditti, J. G., & Church, M. (2020). Experimental Insights into the Threshold of Motion in Alluvial Channels: Sediment Supply and Streambed State. *Journal of Geophysical Research: Earth Surface*, *125*(12). https://doi.org/10.1029/2020JF005736

Herbert, C. M., Alexander, J., & Martínez de Álvaro, M. J. (2015). Back-flow ripples in troughs downstream of unit bars: Formation, preservation and value for interpreting flow conditions. *Sedimentology*, *62*(7), 1814–1836. https://doi.org/10.1111/sed.12203

Hope, J. A., Malarkey, J., Baas, J. H., Peakall, J., Parsons, D. R., Manning, A. J., Bass, S. J., Lichtman, I. D., Thorne, P. D., Ye, L., & Paterson, D. M. (2020). Interactions between sediment microbial ecology and physical dynamics drive heterogeneity in contextually similar depositional systems. Limnology and Oceanography, 1–17. https://doi.org/10.1002/lno.11461

Kim, S.-C., Friedrichs, C. T., Maa, J. P.-Y., & Wright, L. D. (2000). Estimating Bottom Stress in Tidal Boundary Layer from Acoustic Doppler Velocimeter Data. *Journal of Hydraulic Engineering*, *126*(6), 399–406. https://doi.org/10.1061/(asce)0733-9429(2000)126:6(399)

Leckie, S. H. F., Draper, S., White, D. J., Cheng, L., & Fogliani, A. (2015). Lifelong embedment and spanning of a pipeline on a mobile seabed. *Coastal Engineering*, *95*, 130–146. https://doi.org/10.1016/j.coastaleng.2014.10.003

Leckie, S. H. F., Mohr, H., Draper, S., McLean, D. L., White, D. J., & Cheng, L. (2016). Sedimentation-induced burial of subsea pipelines: Observations from field data and laboratory experiments. *Coastal Engineering*, *114*, 137–158. https://doi.org/10.1016/j.coastaleng.2016.04.017

Leckie, S. H. F., Draper, S., White, D. J., Cheng, L., Griffiths, T., & Fogliani, A. (2018). Observed changes to the stability of a subsea pipeline caused by seabed mobility. *Ocean Engineering*, *169*(January), 159–176. https://doi.org/10.1016/j.oceaneng.2018.07.059

Lefebvre, A., Herrling, G., Becker, M., Zorndt, A., Krämer, K., & Winter, C. (2022). Morphology of estuarine bedforms, Weser Estuary, Germany. *Earth Surface Processes and Landforms*, *47*(1), 242–256. https://doi.org/10.1002/esp.5243

Lichtman, I. D., Baas, J. H., Amoudry, L. O., Thorne, P. D., Malarkey, J., Hope, J. A., Peakall, J., Paterson, D.M., Bass, S.J., Cooke, R.D., Manning, A.J., Davies, A.G., Parsons, D.R., Ye, L. (2018). Bedform migration in a mixed sand and cohesive clay intertidal environment and implications for bed material transport predictions. *Geomorphology*, *315*, 17–32. https://doi.org/10.1016/j.geomorph.2018.04.016

MacKenzie, L. G., & Eaton, B. C. (2017). Large grains matter: contrasting bed stability and morphodynamics during two nearly identical experiments. *Earth Surface Processes and Landforms*, *42*(8), 1287–1295. https://doi.org/10.1002/esp.4122

Mayall, R. O., McAdam, R. A., Whitehouse, R. J. S., Burd, H. J., Byrne, B. W., Heald, S. G., et al. (2020). Flume Tank Testing of Offshore Wind Turbine Dynamics with Foundation Scour and Scour Protection. *Journal of Waterway, Port, Coastal, and Ocean Engineering*, *146*(5), 1–17. https://doi.org/10.1061/(asce)ww.1943-5460.0000587

McCarron, C. J., van Landeghem, K. J. J., Baas, J. H., Amoudry, L. O., & Malarkey, J. (2019). The hiding-exposure effect revisited: A method to calculate the mobility of bimodal sediment mixtures. *Marine Geology*, *410*(November 2018), 22–31. https://doi.org/10.1016/j.margeo.2018.12.001

McLean, D., Speed, C. W., Birt, M. J., Colquhoun, J., Case, M., Stowar, M., Bond, T., Ierodiaconou, D., Whitmarsh, S, K., Taylor, M, D., Wines, S., Booth, D, J., Fowler, A, M., Vaughan, B, I. (2022). Habitat value of subsea wells and pipelines for fishery target species in Australia. *Frontiers in Marine Science*, *9*(August), 1–23. https://doi.org/10.3389/fmars.2022.960496

McLean, D. L., Vaughan, B. I., Malseed, B. E., & Taylor, M. D. (2020). Fish-habitat associations on a subsea pipeline within an Australian Marine Park. *Marine Environmental Research*, *153*(October 2019), 104813. https://doi.org/10.1016/j.marenvres.2019.104813

McLean, S. R., Wolfe, S. R., & Nelson, J. M. (1999). Spatially averaged flow over a wavy boundary revisited. *Journal of Geophysical Research: Oceans*, *104*(C7), 15743–15753. https://doi.org/10.1029/1999jc900116

Mohr, H., Draper, S., Cheng, L. & White, D. J. (2016). Predicting the rate of scour beneath subsea pipelines in marine sediments under steady flow conditions. *Coastal Engineering*, 110, 111-126

Nowell, A., & Church, M. A. (1979). Turbulent flow in a depth-limited boundary layer. *Journal of Geophysical Research-Oceans*, *84*(C8), 4816–4824.

Pähtz, T., Clark, A. H., Valyrakis, M., & Durán, O. (2020). The Physics of Sediment Transport Initiation, Cessation, and Entrainment Across Aeolian and Fluvial Environments. *Reviews of Geophysics*. Blackwell Publishing Ltd. https://doi.org/10.1029/2019RG000679

Paterson, D. (1989). Short-term in the erodibility of intertidal cohesive sediments related to the migratory behavior of epipelic diatoms. *Limnology and Oceanography*, *34*(1), 223–234. https://doi.org/10.2307/2837074

Pope, N. D., Widdows, J., & Brinsley, M. D. (2006). Estimation of bed shear stress using the turbulent kinetic energy approach—A comparison of annular flume and field data. *Continental Shelf Research*, *26*(8), 959–970. https://doi.org/10.1016/j.csr.2006.02.010

Rippeth, T. P., Williams, E., & Simpson, J. H. (2002). Reynolds stress and turbulent energy production in a tidal channel. Journal of Physical Oceanography, 32(4), 1242–1251. https://doi.org/10.1175/1520-0485(2002)032<1242:RSATEP>2.0.CO;2

van Rijn, L. (1993). *Principles of Sediment Transport in Rivers, Estuaries and Coastal Seas*. Aqua Publications.

Soulsby, R. (1997). *Dynamics of Marine Sands.* London, UK: Thomas Telford Publications.

Soulsby, R. L., & Dyer, K. R. (1981). The form of the near-bed velocity profile in a tidally accelerating flow. *Journal of Geophysical Research*, *86*(C9), 8067. https://doi.org/10.1029/JC086iC09p08067

Sumer, B M, Truelsen, C., Sichmann, T., & Fredsøe, J. (2001a). *Onset of scour below pipelines and self-burial*. *Coastal Engineering* (Vol. 42).

Sumer, B. M, Whitehouse, R. J. S., & Tørum, A. (2001b). Scour around coastal structures: A summary of recent research. *Coastal Engineering*, *44*(2), 153–190. https://doi.org/10.1016/S0378-3839(01)00024-2

Sumer, B M, & Fredsøe, J. (2001). Scour Around Pile in Combined Waves and Current. *Journal of Hydraulic Engineering*, *127*(5), 403–411.

Sumer, B. M, & Kirca, V. S. O. (2022). Scour and liquefaction issues for anchors and other subsea structures in floating offshore wind farms: A review. *Water Science and Engineering*, *15*(1), 3–14. https://doi.org/10.1016/j.wse.2021.11.002

Sumer, M., & Fredsøe, J. (2002). *The Mechanics of Scour in the Marine Environment* (Vol. 17). World Scientific.

Thompson, C. E. L., Couceiro, F., Fones, G. R., Helsby, R., Amos, C. L., Black, K., et al. (2011). In situ flume measurements of resuspension in the North Sea. *Estuarine, Coastal and Shelf Science*, *94*(1), 77–88. https://doi.org/10.1016/j.ecss.2011.05.026

Thorne, P. D., & Meral, R. (2008). Formulations for the scattering properties of suspended sandy sediments for use in the application of acoustics to sediment transport processes. *Continental Shelf Research*, *28*(2), 309–317. https://doi.org/10.1016/j.csr.2007.08.002

Underwood, G. J. C., & Paterson, D. M. (1993). Seasonal changes in diatom biomass, sediment stability and biogenic stabilization in the Severn Estuary. *Journal of the Marine Biological Association of the United Kingdom*, *73*(4), 871–887. https://doi.org/10.1017/S0025315400034780

Unsworth, C. A., Parsons, D. R., Hardy, R. J., Reesink, A. J. H., Best, J. L., Ashworth, P. J., & Keevil, G. M. (2018). The Impact of Nonequilibrium Flow on the Structure of Turbulence Over River Dunes. *Water Resources Research*, *54*(9), 6566–6584. https://doi.org/10.1029/2017WR021377

Vericat, D., Batalla, R. J., & Garcia, C. (2006). Breakup and reestablishment of the armour layer in a large gravel-bed river below dams: The lower Ebro. *Geomorphology*, *76*(1–2), 122–136. https://doi.org/10.1016/j.geomorph.2005.10.005

Whitehouse, R. J. S. & Draper, S. (2020). Sediment transport and scour in the ocean environment – knowledge and future directions. *Proceedings of the 4th International Symposium on Frontiers in Offshore Geotechnics, ISFOG*, Editor: Zack Westgate. pp 178-205. Deep Foundations Institute.

Williams, J. J., Rose, C. P., Thorne, P. D., O'Connor, B. A., Humphery, J. D., Hardcastle, P. J., et al. (1999). Field observations and predictions of bed shear stresses and vertical suspended sediment concentration profiles in wave-current conditions. *Continental Shelf Research*, *19*(4), 507–536. https://doi.org/10.1016/S0278-4343(98)00098-3

Zhang, J., Chen, Y., Jia, F., Zhou, Y., Li, H., Li, C., Huang, X and Guo, Q (2021). Damage analysis of suspended submarine cable under current force based on finite element simulation. In *ICSMD 2021 - 2nd International Conference on Sensing, Measurement and Data Analytics in the Era of Artificial Intelligence*. Institute of Electrical and Electronics Engineers Inc. https://doi.org/10.1109/ICSMD53520.2021.9670552

Zhao, F., Griffiths, T., Shen, W., Draper, S., An, H., Leggoe, J., & Carneiro, D. (2015). Sediment attractors: Seabed shear stress shadows around subsea pipelines cause net sediment accretion. In *Proceedings of the ASME 2015 34th International Conference on Ocean, Offshore and Arctic Engineering* (p. 13). St John's, Newfoundland.